Michigan State University

National Superconducting Cyclotron Laboratory

FINAL-STATE COULOMB INTERACTIONS FOR INTERMEDIATE-MASS FRAGMENT EMISSION

Y.D. KIM, R.T.de SOUZA, C.K. GELBKE, W.G. GONG, and S. PRATT

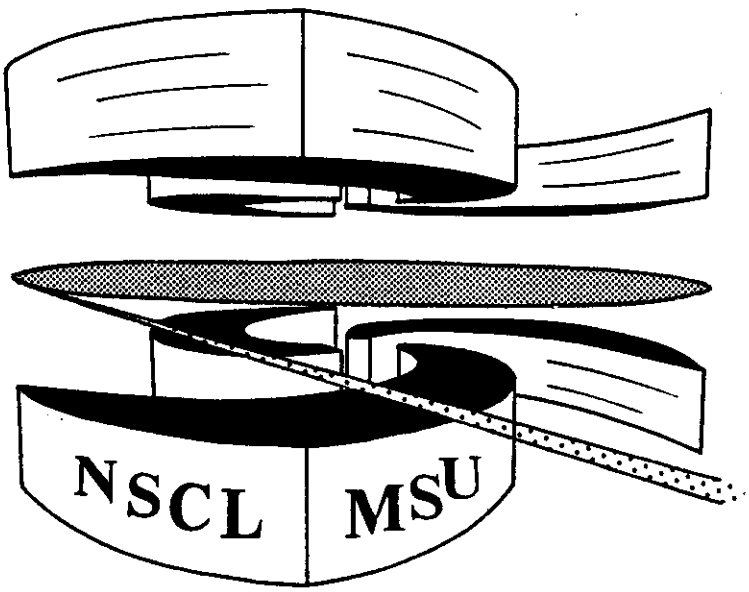

MSUCL-782

JUNE 1991

MSUCL-782
June, 1991

"Final-state Coulomb interactions for intermediate-mass fragment rlasfon"

Y.D. Kim, R.T. de Souza, C.K. Gelbke, W.G. gong

National Superconductlng Cyclotron Laboratory

and Department of Physics and Astronomy

Michigan State University, East Lansing, HI. 48824, USA

S. Pratt

Department of Physics, University of Wisconsin, Madison, WI 63708, USA

Abstract: Information about the space-time characteristics'of Intermediate mass fragment emission processes is contained In the shape of two-fragment correlation functions at small relative momenta. A classical approximation to the Koonln-Pratt formula is derived which allows the calculation of correlations resulting from the Coulcnnb Interaction between the two detected fragments. Distortions in the Coulomb field of heavy reaction residues are evaluated by means of three-body Coulomb trajectory calculations.

PACS index: 25.70.Gh, 25.70.Lm, 25.70.Np

I. Introduction

Highly excited nuclear systems can be produced in intermediate-energy nucleus-nucleus collisions. As the excitation energy is raised from below 1 MeV per nucleon up to about 10 MeV per nucleon, decays by intermediate mass fragment (IMF) emission are predicted and observed to become important [1-57]. Model calculations predict that such highly excited nuclear systems can expand either through the action of thermal pressure [1-4,37,39] or through a dynamical compression-decompression cycle [1,5-12]. If nuclear matter expands to sufficiently low densities, it becomes unstable and density fluctuations can grow exponentially as a function of time [1]. Given enough time, the growth of these fluctuations can cause a multifragment breakup [5-12]. Calculations suggest that the probability for multifragment breakup may be sensitive to the nuclear equation of state at low density [13]. Therefore, information about the equation of state and the liquid-gas phase transition of dilute nuclear matter may be obtainable from detailed studies of multifragment emission processes [5-7,9,14-16,43-45]. Semiclassical computer simulations of the reaction dynamics, on the other hand, suggest that multifragment decays could be caused by dynamical fluctuations rather than by thermodynamic instabilities [17].

At present, a full theoretical understanding of multifragmentation processes in finite nuclear systems is not available and alternative models for multifragment emission processes have been proposed, ranging from static thermodynamical treatments [18-33] to rate-equation approaches based on generalizations of compound-nucleus decay models [34-41]. Additional experimental information is clearly necessary to discriminate between the

various theoretical approaches. Of particular interest are observables which are sensitive to the time scale on which multifragment emissions occur.

When two particles are emitted in close proximity and with small relative momenta, their relative wave-function is affected by final state interactions and, for identical particles, by quantum statistics. Therefore, two-particle correlation functions at small relative momenta are sensitive to the space-time evolution of the emitting system [58-62]. When interactions with the residual system can be neglected, the two-particle correlation functions depend essentially on the single-particle phase space density of the emitted particles [60-62]. Up to now, quantitative comparisons of experimental correlation functions with predictions from specific reaction models have largely been performed for the case of two-proton correlation functions. Rather gratifying agreement between theory and experiment was found for emission processes occurring on rather different time scales. Two-proton correlation functions measured for evaporative emission from equilibrated reaction residues could be understood in terms of slow emission time scales predicted by compound nucleus decay models [63-68]. Two-proton correlation functions measured for non-compound emission processes were found to be in good agreement with the space-time evolution of the reaction zone as predicted by the Boltzmann-Uehling-Uhlenbeck equation [68,69].

While the time scales of nucleon emission processes appear to be reasonably well understood, those governing the emission of intermediate mass fragments in energetic nucleus-nucleus collisions are much less certain and subject to controversial interpretations [28,54]. In this paper, we explore the sensitivity of correlations between two intermediate mass fragments to the

emission time scales. For this purpose, we apply the formalism of refs. [60-62] to the calculation of two-fragment correlation functions resulting from the final-state Coulomb interaction between the two detected fragments. To a high degree of accuracy, such correlations can be treated classically. In many cases of practical interest, the fragments are emitted in the vicinity of a heavy reaction residue. In such cases, the neglect of Coulomb interactions with the residual system may not be justified. In order to assess the effects of distortions in the Coulomb field of the residual system, we will also present correlation functions calculated by means of three-body trajectory calculations. To allow reference to work of ref. [70], we present calculations for correlation functions between intermediate mass fragments of $Z \approx 6$ emitted from heavy composite systems ($Z \approx 93$).

The paper is organized as follows. In Section II, we give a brief derivation of the classical approximation to the formalism of ref. [62], treating only the Coulomb interaction between the two detected fragments. In Section III, we compare longitudinal, transverse, and angle-averaged correlation functions, calculated with the generalized Koonin-Pratt formula by treating the Coulomb interaction between the two detected particles classically and quantum mechanically. Results of three-body trajectory calculations are presented in Section IV. A summary and conclusion are given in Section V.

II. Classical treatment of Coulomb interaction between the detected fragments

In Subsection A, we give a brief summary of the Koonin-Pratt formula for the two-particle correlation function derived in ref. [62]. In Subsection B, we derive a classical expression for the Coulomb interaction between the two fragments.

A. Summary of Koonin-Pratt formalism

The usual treatment of two-proton correlations at higher energies is based upon the Koonin-Pratt formula. The derivation of this formula is based upon the assumption that the final-state interaction between the two detected protons dominates, that final-state interactions with all remaining particles can be neglected, and that the correlation functions are determined by the two-body density of states as corrected by the interactions between the two particles. The density of states for two particles separated by the relative coordinate $\vec{r}$ and emitted in the asymptotic state characterized by the relative momentum $\vec{q}$ is the square of the relative wave function. If the two fragments are emitted simultaneously with thermal distributions or if the momentum distributions are very broad, as is the case at high energy, this approach provides a near-exact answer provided interactions with third bodies may be neglected. For emission from long-lived compound nuclei, the emission is thermal but far from simultaneous. Furthermore, distortions in the long-range Coulomb field of the residual nucleus might not be negligible, especially for particles emitted with energies close to the exit channel Coulomb barrier. While the Koonin-Pratt formula is expected to be reliable for higher energy collisions which are characterized by rapid disintegrations, its range of validity is less clear when it is applied to less energetic regimes.

The Koonin-Pratt formula allows the calculation of the two-particle correlation function in terms of the single particle phase space distribution and the relative wave function of the emitted particle pair [62]:

$$1+R(\vec{P},\vec{q}) = \int d^3r F_{\vec{P}}(\vec{r}) |\phi(\vec{q},\vec{r})|^2 \ . \qquad (1)$$

Here, $\vec{P}=\vec{p}_1+\vec{p}_2$ is the total momentum of the proton pair and $\Phi(\vec{q},\vec{r})$ is the relative two-particle wave function. Here $\vec{q}=\mu d\vec{r}/dt$ is the relative momentum between the two particles, $\vec{r}$ is the relative coordinate, and $\mu=m_1m_2/(m_1+m_2)$ is the reduced mass. The relative Wigner function $F_{\vec{P}}(\vec{r})$ is defined by:

$$F_{\vec{P}}(\vec{r}) = \frac{\int d^3X f_1(\vec{P}\mu/m_2,\vec{X}+\vec{r}\mu/m_1,t_>)f_2(\vec{P}\mu/m_1,\vec{X}-\vec{r}\mu/m_2,t_>)}{|\int d^3X_1 f_1(\vec{P}\mu/m_2,\vec{X}_1,t_>)\cdot\int d^3X_2 f_2(\vec{P}\mu/m_1,\vec{X}_2,t_>)|} \quad . \tag{2}$$

Here, $\vec{X}$ is the coordinate of the center-of-mass of the fragment pair, $f_1(\vec{p}_1,\vec{r}_1,t_>)$ is the phase-space distribution of particles of type i with momentum $\vec{p}_1$ at position $\vec{r}_1$ at some time $t_>$ after the emission process. If the particles cease to interact at a time earlier than $t_>$, then the relative Wigner function is independent of the particular choice of $t_>$ and the function $f_1(\vec{p}_1,\vec{r}_1,t_>)$ can be expressed in terms of the emission function, $g_1(\vec{p}_1,\vec{r}_1,t)$, i.e. the probability of emitting a particle of type i with momentum $\vec{p}_1$ at location $\vec{r}_1$ and time t [62]:

$$f_1(\vec{p}_1,\vec{r}_1,t_>) = \int_{-\infty}^{t_>} dt\; g_1[\vec{p}_1,\vec{r}_1-\vec{p}_1(t_>-t)/m_1,t] \quad . \tag{3}$$

In this paper, we will use a simple parametrization for the emission functions $g(\vec{p},\vec{r},t)$, corresponding to surface emission from a spherical source of radius R_S with a fixed lifetime τ and a Maxwellian energy distribution characterized by a temperature parameter T:

$$g(\vec{p},\vec{r},t) \propto (\hat{r}\cdot\hat{p})\theta(\hat{r}\cdot\hat{p})\delta(r-R_S)\theta(E-V_C)\sqrt{E-V_C}\; e^{-(E-V_C)/T}\; e^{-t/\tau} \quad . \tag{4}$$

Here, $\theta(x)$ is the unit step function which vanishes for $x<0$, $\delta(x)$ is the delta function, $\hat{r}$ and $\hat{p}$ are unit vectors parallel to $\vec{r}$ and $\vec{p}$, and $E=p^2/2m$. The parameter V_C is introduced to account for Coulomb repulsion when emission occurs from the surface of a heavy reaction residue assumed to be at rest at the origin of our coordinate system.

For calculations of two-fragment correlation functions based upon Eq. 1, we neglect nuclear interactions and assume the particles to be distinguishable. Furthermore, only phase space points are integrated over for which the relative separation between the two fragments is larger than the sum of their radii, $r>1.2(A_1^{1/3}+A_2^{1/3})$ fm. The relative wave function can be calculated by using a partial wave expansion of the Coulomb scattering amplitude. In our quantum mechanical treatment of the two-fragment Coulomb interaction, the number, ℓ_{max}, of partial waves included in the calculations was scaled according to the classical relation $\ell_{max}= 20(h/2\pi)+(q^2r^2-2\eta qr)^{1/2}$, where $\eta=Z_1Z_2\alpha\mu c/q$ is the Sommerfeld parameter and $\alpha=2\pi e^2/hc\approx 1/137$ is the fine structure constant.

B. Classical treatment of two-fragment Coulomb interaction

Calculations based upon Eq. 1 are rather tedious and time consuming [71]. It is, therefore, of interest to derive a classical expression. Again, we assume that the correlation function is the ratio of available states with and without interactions. If $\vec{q}_0$ and $\vec{q}$ denote the initial and final relative momentum vectors, we have:

$$C(\vec{q},\vec{r}_0) \approx \left| \frac{q_0^2 dq_0 \, \sin\theta_0 d\theta_0 \, d\phi_0}{q^2 dq \, \sin\theta d\theta \, d\phi} \right| . \qquad (5)$$

Here, θ_0 and θ denote the angles between the initial relative position vector $\vec{r}_0$ and the initial and final momentum vectors, respectively: $\cos\theta_0=\hat{r}_0\cdot\hat{q}_0$ and $\cos\theta=\hat{r}_0\cdot\hat{q}$. From angular momentum conservation, we have for azimuthal rotations about the axis parallel to $\hat{r}_0$:

$$d\Phi = d\Phi_0 \ . \tag{6}$$

Energy conservation gives the relation

$$q_0^2 = q^2 - 2\mu\kappa/r_0 \ , \tag{7}$$

where $\kappa=Z_1Z_2e^2$ is the product of the charges of the two emitted fragments. From Eq. (6) one immediately obtains

$$q_0^2 dq_0 = (1-2\mu\kappa/q^2r_0)^{1/2}q^2dq \ . \tag{8}$$

By using the fact that the eccentricity vector,

$$\vec{\varepsilon} = \vec{q}\times\vec{L}/\mu\kappa + \hat{r} = \vec{q}\times(\vec{r}\times\vec{q})/\mu\kappa + \hat{r} \ , \tag{9}$$

is a constant of motion and equating its two components in the scattering plane at the time of emission and at very large times, one obtains the following relations:

$$\mu\kappa + r_0q_0^2\sin^2\theta_0 = \mu\kappa\cos\theta + r_0qq_0\sin\theta\sin\theta_0 \ , \tag{10}$$

$$r_0q_0^2\cos\theta_0\sin\theta_0 = r_0qq_0\cos\theta\sin\theta_0 - \mu\kappa\sin\theta \ . \tag{11}$$

Here, we made use of angular momentum conservation and of the fact that the two vectors $\vec{r}$ and $\vec{q}$ become parallel for $t\to\infty$. Equation 10 can be cast into the form:

$$\sin\theta_0 = (q/2q_0)\{\sin\theta \pm [\sin^2\theta - 4\mu\kappa(1-\cos\theta)/r_0q^2]^{1/2}\} \quad . \tag{12}$$

Equation 12 has two solutions: for given final relative momentum $\vec{q}$, there are two different trajectories which pass through the relative coordinate $\vec{r}_0$. Both trajectories must be considered when calculating the correlation function. Equation 11 can be written as:

$$\cos\theta_0 = (q/q_0)\cos\theta - (\mu\kappa/r_0q_0^2)\sin\theta/\sin\theta_0 \quad . \tag{13}$$

Differentiation of Eq. 12 yields:

$$d\theta_0/d\theta = \frac{q}{2q_0\cos\theta_0}\left\{\cos\theta \pm \frac{\cos\theta\sin\theta - 2\mu\kappa\sin\theta/r_0q^2}{[\sin^2\theta - 4\mu\kappa(1-\cos\theta)/r_0q^2]^{1/2}}\right\} \quad . \tag{14}$$

Using Eqs. 7, 12-14, one can express $\sin\theta_0 d\theta_0/\sin\theta d\theta$ in terms of the of the initial relative coordinate r_0 and the asymptotic values of θ and q. Hence, Eqs. 6-8, 12-14 allow the expression of Eq. 5 in terms of the final relative momentum and the initial relative position of the emitted particles. Integration over all relative positions of the emitted particles gives the final expression for the correlation function:

$$1+R(\vec{p},\vec{q}) = \int d^3r_0 F_{\vec{p}}(\vec{r}_0)C(\vec{q},\vec{r}_0) \quad . \tag{15}$$

If all direction of $\vec{q}$ are integrated over, Eq. 5 reduces to a particularly simple expression,

$$C(q,r_0) = (1-2\mu k/q^2 r_0)^{1/2} \quad , \tag{16}$$

which can be used for calculating the angle integrated correlation function R(P,q). Equation 16 indicates that two-fragment correlation functions measured for different particle pairs depend largely on the variable

$$\mu k/q^2 = \mu e^2 Z_1 Z_2/(\mu v_{rel})^2 \propto (Z_1+Z_2)/v_{rel}^2 \quad . \tag{17}$$

In the last step, we have made use of the fact that most intermediate mass fragments are produced close to the valley of stability, i.e. we have approximated $m_1 \propto 2Z_1$. Within this approximation, one can generate two-fragment correlation functions by combining the statistics from several fragment combinations and evaluating the dependence as a function of the "reduced" relative velocity,

$$v_{red} = v_{rel}/\sqrt{Z_1+Z_2} \quad . \tag{18}$$

We will use this variable to display the results of our numerical calculations. The use of the reduced velocity as an independent variable is different from the convention employed in ref. [55] where mixed-fragment correlations were evaluated as a function of relative velocity of the emitted fragments. Close inspection of Eqs. 5-8, 12-14 shows that most of these relations also scale as $\mu k/q^2$, the only exception being Eq. 13 which contains a term which scales as $\mu k/q_0^2$. If dependences on the angle θ are important, scaling of

mixed-fragment correlations with $\mu\kappa/q^2$ is not exact, but it may still be a reasonable approximation.

III. Validity of classical approximation

In this section we assess the validity of the classical approximation, Eqs. 5-8, 12-15. Calculations with these equations are compared to calculations with Eq. 1 in which the full Coulomb scattering wave function is used for the relative wave function. As a specific example, we calculate correlation functions for the emission of two distinguishable carbon nuclei, using emission functions of the form of Eq. 4. In these calculations we kept the parameters T=15 MeV, R_S=12 fm, V_C= 63 MeV fixed and varied the lifetimes τ as indicated in the figures.

Figure 1 gives a comparison of correlation functions integrated over all relative orientation between the total and relative momenta of the two emitted fragments. The points show calculations with Eq. 1 and the curves show results obtained with the classical expression, Eqs. 15 and 16. The two calculations produce virtually identical results indicating that the classical approximation is very well justified. (Some small differences exist at large relative velocities for the calculations with τ=500 fm/c; these are due to the limitation in the number of partial waves used in our calculations with Eq. 1.)

In Fig. 2, calculations for longitudinal and transverse correlation functions are compared for τ=200 fm/c. These correlation functions are defined in terms of the angle Ψ between $\vec{P}$ and $\vec{q}$, $\Psi=\cos^{-1}(\vec{P}\cdot\vec{q}/Pq)$. Longitudinal correlation functions correspond to the angular interval Ψ=0°-30° or Ψ=150°-180°;

transverse correlation functions correspond to the angular interval Ψ=80°-100°. The curves show the results obtained with Eq. 1 and the points show the results obtained with the classical relations, Eqs. 5-8, 12-15. Again, the two calculations produce virtually identical results. We conclude that classical treatments of correlation functions between intermediate mass fragments provide an excellent approximation. The validity of the classical approximation is, of course, expected for emission from sources with dimensions comparable to or larger than the Bohr radius. For the two-carbon system the Bohr radius is 0.13 fm which is, indeed, much smaller than the size of the emitting system.

For emission from long-lived systems, longitudinal correlation functions are predicted to exhibit a wider minimum at $q \approx 0$ than transverse correlation functions. This directional dependence is due to the fact that the Coulomb force is parallel to the relative displacement of the particles. Therefore, the Coulomb hole in the correlation function will be strongest when the relative momentum is parallel to the longest dimension of the pair's separation. For long-lived sources this is the longitudinal direction [61,62].

IV. Trajectory calculations

The derivation of Eq. 1 is based upon the assumptions that the phase space distribution does not vary significantly over the range $\frac{1}{2}P \pm q$ and, furthermore, that dynamical correlations and distortions in the Coulomb field of other reaction residues can be neglected. In this section we assess the validity of these assumptions by means of trajectory calculations. The use of trajectory calculations is justified by the validity of the classical approximation.

In our trajectory calculations we consider the sequential emission of two carbon nuclei from the surface of a source of radius R_S which is initially at rest and which has a total charge of $Q_S=Z_S e=93e$ and a total mass of $M_S=A_S$ u. In order to isolate the effect of three body Coulomb distortions from dynamic distortions resulting from the recoil of the emitting system, we use an artificially large mass number for the emitting source, $A_S=10000$. Further below, we evaluate recoil effects for a more realistic heavy source of mass number $A_S=226$. To be consistent with the calculations presented in Section III, we assumed an emission function of the form:

$$g(\vec{p},\vec{r},t) \propto (\hat{r}\cdot\hat{p})\theta(\hat{r}\cdot\hat{p})\delta(r-R_S)\theta(E)\sqrt{E}\, e^{-E/T}\, e^{-t/\tau} \quad . \tag{19}$$

This emission function was sampled by Monte-Carlo techniques. For the emission of a second fragment, we imposed the additional requirement that the second fragment had a minimum initial separation of $r>1.2(A_1^{1/3}+A_2^{1/3})$ fm from the first fragment. Upon emission, the particle trajectories were calculated by integrating Newton's equations, and the asymptotic particle momenta were stored as coincidence events and as single-particle spectra. Correlation functions, 1+R, were constructed from the calculated coincidence and single-particle yields, $Y_{12}(\vec{p}_1,\vec{p}_2)$ and $Y_1(\vec{p}_1)$, respectively:

$$\Sigma Y_{12}(\vec{p}_1,\vec{p}_2) = C[1+R(q)]\Sigma Y_1(\vec{p}_1)Y_2(\vec{p}_2) \quad . \tag{20}$$

Here, $\vec{p}_1$ and $\vec{p}_2$ are the laboratory momenta of fragments 1 and 2; $\vec{q}=\mu\vec{v}_{rel}$ is the relative momentum of the particle pair, and C is a normalization constant determined by the requirement that $\langle R(q)\rangle=0$ at large relative momenta where the final state interaction between the emitted fragments can be neglected.

For each gating condition on P and $\Psi=\cos^{-1}(\hat{q}\cdot\hat{P})$, the correlation function was evaluated by summing both sides of Eq. 20 over all momentum combinations corresponding to given values of q (or v_{red}). The parameters used in our calculations were chosen to be consistent with those used for the calculations presented in the previous section, T=15 MeV and R_S=12 fm. The emission times are indicated in the figures.

First, we explore the validity of using the approximate form of the phase space distribution, Eq. 2. For this purpose we have performed trajectory calculations in which the Coulomb interaction with the emitting source was turned off. In Fig. 3, the results of these calculations are compared to calculations based upon Eq. 15 and 16 (these latter calculations are identical with results obtained from Eq. 1). The open points represent the results obtained from these trajectory calculations and the curves show the results obtained from Eqs. 15 and 16. The difference between the two calculations is significant, but not necessarily surprising. The emission function varies over characteristic momenta of the order of $\Delta p \approx \sqrt{2mT} \approx 0.6$ GeV/c. The Coulomb minimum of the two-fragment correlation function has a width of the order of $\Delta q \approx 0.2$-0.3 GeV/c. Hence, the condition $\Delta q << \Delta p$ is only poorly satisfied. It is somewhat better satisfied for large values of τ than for small values of τ. Therefore, the agreement between the two calculations becomes better for larger lifetimes. According to the above arguments, the discrepancy between trajectory calculations and calculations based upon Eqs. 1 or 15 should become less for larger slope parameters T used to characterize the energy spectra. This expectation is borne out in the calculations shown by the solid points in Fig. 4, which were performed for the extreme limit of flat energy spectra, $T=\infty$, for two ranges of the total momentum P of the particle pair. For the emission of

energetic fragments, P/A≥150 MeV/c, reasonable agreement exists with results from the Koonin-Pratt formula (upper panel of Fig. 4). However, for low-energy fragments, P≤140 MeV/c, the discrepancies are still considerable (lower panel of Fig. 4).

We now address distortions in the Coulomb field of heavy reaction residues of total charge number Z_S=93, still neglecting recoil effects by setting the mass of the emitting source to M_S=10000 u. In Fig. 5, we explore the scaling of the two-fragment correlation functions with the reduced relative velocity, Eq. 18. In these calculations we used the parameters T=15 MeV and τ=200 fm/c. One fragment was assumed to be carbon (Z_1=6) and the other fragment was taken as a fragment of element number Z_2=4-9. The sequence of emission between fragments 1 and 2 was chosen randomly. For the mass number of the emitted fragments we assumed A=2Z. In the upper panel of the figure, the correlation functions are displayed as a function of relative momentum q. As expected, the minimum at q≠0 becomes wider as the charge of the second fragment is increased. The lower part of the figure shows the dependence of the calculated correlation functions as a function of the reduced relative velocity. The scaling of the calculated correlation functions with the reduced velocity of the emitted fragment pair is rather well preserved. Such scaling can be of significant practical importance since considerable improvements in statistical accuracy can be gained from two-fragment correlation functions integrated over many fragment combinations. For orientation, the curves show calculations with Eqs. 15 and 16. While these calculations do not accurately reproduce the shape of the correlation functions obtained via trajectory calculations, they are still useful in providing a first estimate of the lifetime of the emitting system.

In Fig. 6 we compare two-carbon correlation functions calculated by means of trajectory calculations (points) with correlation function calculated with Eqs. 15 and 16 (curves). The upper and lower panels show the results for carbon pairs emitted with total momenta per nucleon, P/A≤110 MeV/c and P/A≥110 MeV/c, respectively. For the low momentum gate, the fragments are emitted with very small initial velocities and distortions in the Coulomb field of the emitting source should be maximal. Indeed, significant distortions already exist for τ=200 fm/c. For longer emission times, calculations with Eq. 15 and 16 can still provide useful guidance, as is illustrated by the good agreement with the trajectory calculations for τ=500 fm/c. However, for shorter lifetimes ($\tau \lesssim 200$ fm/c) distortions in the Coulomb field of the emitting source become so large that Eqs. 15 and 16 become virtually useless. As may be expected, distortions by the Coulomb field of the emitting system are less important for fragment pairs emitted with larger initial velocities. This qualitative expectation is borne out by the calculations for more energetic fragment pairs with P/A≥110 MeV/c. For this momentum gate, Eqs. 15 and 16 provide reasonable approximations for emission times $\tau \gtrsim 200$ fm/c. However, for shorter emission times, the disagreement is still substantial, though much smaller than for the low-momentum gate.

For the emission of rather energetic particles, three-body Coulomb distortions of the angle averaged correlation functions become small, even for rather short emission times. As an example, the open points in Fig. 4 show the results of three-body Coulomb trajectory calculations performed for flat energy spectra, T=∞, and for Z_S=93. For energies well above the Coulomb barrier, P/A≥150 fm/c, the distortions in the field of the emitting source become small and trajectory calculations (for Z_S=0 as well as Z_S=93) agree

nearly quantitatively with calculations performed with Eqs. 15 and 16 even for emission time scales as small as τ=50 fm/c. However for low-energy emissions, P/A$\leq$140 MeV/c, the discrepancies are appreciable. It is interesting to note that three-body Coulomb distortions and inaccuracies of the Koonin-Pratt formula for Z_S=0 appear to become small at comparable energies.

Distortions in the Coulomb field of the emitting system can be particularly large for longitudinal and transverse correlation functions. As an example, Fig. 7 shows longitudinal and transverse correlation functions for a relatively long lifetime, τ=200 fm/c. For this lifetime, angle integrated correlation functions calculated via trajectory calculations still exhibit reasonable scaling with the reduced velocity (Fig. 5), and deviations from the calculations with Eqs. 1 or 15 are still relatively modest (Fig. 6). In order to increase statistics, we had to widen the angular acceptance for the longitudinal correlation function, Ψ=0°-50° or 130°-180°. (In the present simulation, the energy spectra are relatively strongly peaked at the Coulomb barrier. As a consequence, only relatively few events in the longitudinal gate fall into the region of relative velocities of interest here.) The longitudinal (circular points) and transverse (square shaped points) correlation functions deduced from the trajectory calculations were normalized with the same normalization constant determined from the asymptotic behavior of the angle integrated correlation function. Although the statistical errors for the longitudinal correlation function are large, it is clear that it exhibits a narrower minimum at $v_{red}\approx 0$ than the transverse correlation function, in complete disagreement with the qualitative trends predicted from Eqs. 1 or 15, see Fig. 2. Hence, the detailed shape of longitudinal and transverse two-fragment correlation functions can be strongly affected by residual

interactions with the Coulomb field of the residual system. It would be of interest to investigate whether such sensitivities to the charge distribution of the emitting system could be exploited to differentiate between various reaction models for multifragment disintegrations.

Since intermediate mass fragments are emitted with larger average momenta than light particles, one may expect that two-fragment correlation functions can also be affected by dynamical correlations due to momentum conservation effects. In Fig. 8, we assess the magnitude of distortions resulting from the recoil of heavy reaction residues. The solid points in the figure show three-body trajectory calculations for emission from a realistic source of mass M_S=226 u and the open points show the results for emission from an artificially heavy source of mass M_S=10000 u for which recoil effects are negligible. The upper panel shows calculations for thermal energy spectra with T=15 MeV and the lower panel shows calculations for flat energy spectra, T=∞, averaged over a broad range of energies E_1, E_2 = 63-563 MeV; other parameters of the calculation were kept fixed (R_S=12 fm, Z_S=93, τ=200 fm/c). For the calculations with T=15 MeV, recoil effects introduce only minor distortions, largely because most particle are emitted with energies close to the Coulomb barrier. For the emission of more energetic fragments, recoil effects become slightly more important as is illustrated by the calculations for T=∞, shown in the bottom panel of Fig. 8. Our schematic investigation is aimed at emission from rather heavy nuclear systems. For lighter sources, of course, recoil effects become more important. One must stress, however, that reasonably unambiguous assessments of recoil effects can only be made within the framework of specific reaction models, particularly for fast noncompound emission processes expected to set in at higher energies.

V. Summary and Conclusion

In this paper, we investigated correlations between two intermediate mass fragments resulting from final-state Coulomb interactions. Such correlations are of interest since the interaction is well understood and since classical treatments provide an excellent approximation. The schematic model calculations presented in this paper indicate that two-fragment correlation functions are, indeed, sensitive to the space-time evolution of the emitting system. However, for emissions occuring on fast time scales and with low kinetic energies, the shape of the correlation functions can be strongly affected by interactions with the residual system thus rendering the interpretation of experimental two-fragment correlation functions dependent on the charge distribution of the remaining particles.

For large emission times ($\tau \gtrsim 200$ fm/c) and fragment kinetic energies well above the Coulomb barrier, calculations incorporating the mutual Coulomb interaction between the two emitted fragments allow the extraction of emission time scales with reasonable accuracy. Within this approximation, the correlation functions depend primarily on the reduced relative fragment velocity, $v_{red} \propto v_{rel}\sqrt{\mu/Z_1Z_2} \propto v_{rel}/\sqrt{Z_1+Z_2}$, provided that the various fragments are emitted from sources of similar space-time geometries. Such scaling allows the measurement of mixed-fragment correlation functions with significantly improved statistical accuracy and with minimal loss of resolution, provided that distortions due to three-body or higher-order interactions do not become prohibitively large.

For emission from heavy and highly charged systems, distortions from interactions with the Coulomb field of the residual system can be significant

thus rendering the analysis more model dependent. Such distortions are particularly important for fragment emission with low kinetic energies or on fast emission time scales. Additional model dependences can arise from dynamical correlations resulting, for example, from momentum conservation.

Directional dependences of two-fragment correlation functions are particularly sensitive to final-state Coulomb interactions with the residual system. Indeed, the shapes of longitudinal and transverse correlation functions can be strongly altered by interactions with the Coulomb field of the emitting system, even when the angle-integrated correlation functions appear to suffer only minor distortions. Such enhanced sensitivities of two-fragment correlation functions to properties of the emitting system may contain useful additional information on the emission process and thus allow more stringent tests for various models for multifragment disintegrations. Thus it appears promising to pursue more detailed calculations of two-fragment correlation functions for specific reaction models capable of making predictions of the space-time evolution of nuclear disintegrations by multi-fragment emission.

This work is based upon work supported by the National Science Foundation under Grant number PHY-89-13815.

References

1. G. Bertsch and P.J. Siemens, Phys. Lett. 126B, 9 (1983).
2. H. Sagawa and G.F. Bertsch, Phys. Lett. 155B, 11 (1985).
3. H. Schulz, D.N. Voskresensky, and J. Bondorf, Phys. Lett. 147B, 17 (1984).
4. S. Levit and P. Bonche, Nucl. Phys. A437, 426 (1984).
5. A. Vicentini, G. Jacucci, and V.R. Pandariphande, Phys. Rev. C31, 1783 (1985).
6. R.J. Lenk and V.R. Pandharipande, Phys. Rev. C34, 177 (1986).
7. T.J. Schlagel, and V.R. Pandharipande, Phys. Rev. C36, 162 (1987).
8. W. Bauer, G.F. Bertsch, and S. Das Gupta, Phys. Rev. Lett. 58, 863 (1987).
9. K. Sneppen, and L. Vinet, Nucl. Phys. A480, 342 (1988).
10. J. Aichelin, G. Peilert, A. Bohnet, A. Rosenhauer, H. Stöcker, and W. Greiner, Nucl. Phys. A488, 437c (1988).
11. G. Peilert, H. Stöcker, W. Greiner, A. Rosenhauer, A. Bohnet, and J. Aichelin, Phys. Rev. C39, 1402 (1989).
12. D.H. Boal and J.N. Glosli, Phys. Rev. C37, 91 (1988).
13. E. Suraud, Nucl. Phys. A495, 73 (1989).
14. X. Campi, Phys. Lett. B208, 351 (1988).
15. W. Bauer, Phys. Rev. C38, 1297 (1988).
16. C. Ngô, H. Ngô, S. Leray, and M.E. Spina, Nucl. Phys. A499, 148 (1989).
17. D.H. Boal and J. Glosli, Phys. Rev. C42, R502 (1990).
18. J. Randrup and S. Koonin, Nucl. Phys. A356, 223 (1981).
19. G. Fai and J. Randrup, Nucl. Phys. A381, 557 (1982).
20. G. Fai and J. Randrup, Phys. Lett. 115B, 281 (1982).
21. G. Fai and J. Randrup, Nucl. Phys. A404, 281 (1983).
22. D.H.E. Gross, L. Satpathy, T.C. Meng, and M. Satpathy, Z. Phys. A309, 41 (1982).

23. D.H.E. Gross and X.Z. Zhang, Phys. Lett. 161B, 47 (1985).

24. Sa Ban-Hao and D.H.E. Gross, Nucl. Phys. A437, 643 (1985).

25. D.H.E. Gross, X.Z. Zhang, and S.Y. Xu, Phys. Rev. Lett. 56, 1544 (1986).

26. X.Z. Zhang, D.H.E. Gross, S.Y. Xu, and Y.M. Zheng, Nucl. Phys. A461, 641 (1987).

27. X.Z. Zhang, D.H.E. Gross, S.Y. Xu, and Y.M. Zheng, A461, 668 (1987).

28. D.H.E. Gross, Phys. Lett. B203, 26 (1988).

29. J.P. Bondorf, R. Donangelo, I.N. Mishustin, C.J. Pethick, H. Schulz, and K. Sneppen, Nucl. Phys. A443, 321 (1985).

30. J.P. Bondorf, R. Donangelo, I.N. Mishustin, and H. Schulz, Nucl. Phys. A444, 460 (1985).

31. J.P. Bondorf, R. Donangelo, I.N. Mishustin, C.J. Pethick, and K. Sneppen, Phys. Lett. 150B, 57 (1985);

32. J.P. Bondorf, R. Donangelo, H. Schulz, and K. Sneppen, Phys. Lett. 162B, 30 (1985).

33. R. Donangelo, K. Sneppen, and J.P. Bondorf, Phys. Lett. B219, 165 (1989).

34. L.G. Moretto, Nucl. Phys. A247, 211 (1975).

35. W.A. Friedman and W.G. Lynch, Phys. Rev. C28, 950 (1983).

36. L.G. Moretto and G. Wozniak, Prog. Part. and Nucl. Phys. 38, 401 (1988).

37. W.A. Friedman, Phys. Rev. Lett. 60, 2125 (1988).

38. W.A. Friedman, Phys. Rev. C40, 2055 (1989).

39. W.A. Friedman, Phys. Rev. C42, 667 (1990).

40. C. Barbagallo, J. Richert, and P. Wagner, Z. Phys. A324, 97 (1986).

41. J. Richert and P. Wagner, Nucl. Phys, A517, 399 (1990).

42. W. Lynch, Ann. Rev. Nucl. Part. Sci., 37, 493 (1987); and references contained therein.

43. J.E. Finn, S. Agarwal, A. Bujak, J. Chuang, L.J. Gutay, A.S. Hirsch, R.W. Minich, N.T. Porile, R.P. Scharenberg, B.C. Stringfellow, and F. Turkot, Phys. Rev. Lett. 49, 1321 (1982).

44. A.S. Hirsch, A. Bujak, J.E. Finn, L.J. Gutay, R.W. Minich, N.T. Porile, R.P. Scharenberg, B.C. Stringfellow, and F. Turkot, Phys. Rev. C29, 508 (1984).

45. A.D. Panagiotou, M.W. Curtin, H. Toki, D.K. Scott, and P.J. Siemens, Phys. Rev. Lett. 52, 496 (1984).

46. C.B. Chitwood, D.J. Fields, C.K. Gelbke, W.G. Lynch, A.D. Panagiotou, M.B. Tsang, H. Utsunomiya and W.A. Friedman, Phys. Lett. 131B, 289 (1983).

47. L.G. Sobotka, M.A. McMahan, R.J. McDonald, C. Signarbieux, G.J. Wozniak, M.L. Padgett, J.H. Gu, Z.H. Liu, Z.Q. Yao, and L.G. Moretto. Phys. Rev. Lett. 53, 2004 (1984).

48. D.J. Fields, W.G. Lynch, C.B. Chitwood, C.K. Gelbke, M.B. Tsang, H. Utsunomiya and J. Aichelin, Phys. Rev. C30, 1912 (1984).

49. D.J. Fields, W.G. Lynch, T.K. Nayak, M.B. Tsang, C.B. Chitwood, C.K. Gelbke, R. Morse, J. Wilczynski, T.C. Awes, R.L. Ferguson, F. PLasil, F.E. Obenshain, and G.R. Young, Phys. Rev. C34, 536 (1986).

50. B.V. Jacak, G.D. Westfall, G.M. Crawley, D. Fox, C.K. Gelbke, L.H. Harwood, B.E. Hasselquist, W.G. Lynch, D.K. Scott, H. Stöcker, M.B. Tsang, G. Buchwald, and T.J.M. Symons, Phys. Rev. C35, 1751 (1987).

51. D.E. Fields, K. Kwiatkowski, D. Bonser, R.W. Viola, V.E. Viola, W.G. Lynch, J. Pochodzalla, M.B. Tsang, C.K. Gelbke, D.J. Fields, and S.M. Austin, Phys. Lett. B220, 356 (1989).

52. J.W. Harris, B.V. Jacak, K.H. Kampert, G. Claesson, K.G.R. Doss, R. Ferguson, A.I. Gavron, H.A. Gustafsson, H. Gutbrod, B. Kolb, F. Lefebvres, A.M. Poskanzer, H.G. Ritter, H.R. Schmidt, L. Teitelbaum, M. Tincknell, S. Weiss, H. Wieman, and J. Wilhelmy, Nucl. Phys. A471, 241c (1987).

53. K.G.R. Doss, H.A. Gustafsson, H. Gutbrod, J.W. Harris, B.V. Jacak, K.H. Kampert, A.M. Poskanzer, H.G. Ritter, H.R. Schmidt, L. Teitelbaum, M. Tincknell, S. Weiss, and H. Wieman, Phys. Rev. Lett. 59, 2720 (1987).

54. D.R. Bowman, W.L. Kehoe, R.J. Charity, M.A. McMahan, A. Moroni, A. Bracco, S. Bradley, I. Iori, R.J. McDonald, A.C. Mignerey, L.G. Moretto, M.N. Namboodiri, and G.J. Wozniak, Phys. Lett. B189, 282 (1987).

55. R. Trockel, U. Lynen, J. Pochodzalla, W. Trautmann, N. Brummund, E. Eckert, R. Glasow, K.D. Hildenbrand, K.H. Kampert, W.F.W. Müller, D. Pelte, H.J. Rabe, H, Sann, R. Santo, H. Stelzer, and R. Wada, Phys. Rev. Lett. 59, 2844 (1987).

56. Y.D. Kim, M.B. Tsang, C.K. Gelbke, W.G. Lynch, N. Carlin, Z. Chen, R. Fox, W.G. Gong, T. Murakami, T.K. Nayak, R.M. Ronningen, H.M. Xu, F. Zhu, W. Bauer, L.G. Sobotka, D. Stracener, D.G. Sarantites, Z. Majka, V. Abenante, and H. Griffin, Phys. Rev. Lett. 63, 494 (1989).

57. Y. Blumenfeld, N. Colonna, P. Roussel-Chomaz, D.N. Delis, K. Hanold, J.C. Meng, G.F. Peaslee, G.J. Wozniak, L.G. Moretto, B. Libby, G. Guarino, N. Santoruvo, and I. Iori, Phys. Rev. Lett. 66, 576 (1991).

58. For a recent review, see e.g. D.H. Boal, C.K. Gelbke, and B.K. Jennings, Rev. Mod. Phys. 62, 553 (1990).

59. G.I. Kopylov and M.I. Podgoretskii, Sov. J. Nucl. Phys. 15, 219 (1972).

60. S.E. Koonin, Phys. Lett. 70B, 43 (1977).

61. S. Pratt and M.B. Tsang, Phys. Rev. C36, 2390 (1987).

62. W.G. Gong, W.Bauer, C.K. Gelbke, and S. Pratt, Phys. Rev. C43, 781 (1991).

63. P.A. DeYoung, M.S. Gordon, Xiu qin Lu, R.L. McGrath, J.M. Alexander, D.M. de Castro Rizzo, and L.C. Vaz, Phys. Rev. C39, 128 (1989).

64. P.A. DeYoung, C.J. Gelderloos, D. Kortering, J. Sarafa, K. Zienert, M.S. Gordon, B.J. Fineman, G.P. Gilfoyle, X. Lu, R.L. McGrath, D.M. de Castro

Rizzo, J.M. Alexander, G. Auger, S. Kox, L.C. Vaz, C. Beck, D.J. Henderson, D.G. Kovar, and M.F. Vineyard, Phys. Rev. C41, R1885 (1990).

65. J. Québert, R. Boisgard, P. Lautridou, D. Ardouin, D. Durand, D. Goujdami, F. Guilbault, C. Lebrun, R. Tamisier, A. Péghaire, and F. Saint-Laurent, Proceedings of the Symposium on Nuclear Dynamics and Nuclear Disassembly, held at Dallas, April 1989, edited by J.B. Natowitz, World Scientific, Singapore 1989, p. 337.

66. D. Ardouin, F. Guilbault, C. Lebrun, D. Ardouin, S. Pratt, P. Lautridou, R. Boisgard, J. Québert, and A. Péghaire, University of Nantes, Internal Report LPN-89-02.

67. W.G. Gong, C.K. Gelbke, N. Carlin, R.T. de Souza, Y.D. Kim, W.G. Lynch, T. Murakami, G. Poggi, D. Sanderson, M.B. Tsang, H.M. Xu, D.E. Fields, K. Kwiatkowski, R. Planeta, V.E. Viola, Jr., S.J. Yennello, and S. Pratt, Phys. Lett. B246, 21 (1990).

68. W.G. Gong, C.K. Gelbke, W. Bauer, N. Carlin, R.T. de Souza, Y.D. Kim, W.G. Lynch, T. Murakami, G. Poggi, D.P. Sanderson, M.B. Tsang, H.M. Xu, D.E. Fields, K. Kwiatkowski, R. Planeta, V.E. Viola, Jr., S.J. Yennello, and S. Pratt, Phys. Rev. C43, 1804 (1991).

69. W.G. Gong, W. Bauer, C.K. Gelbke, N. Carlin, R.T. de Souza, Y.D. Kim, W.G. Lynch, T. Murakami, G. Poggi, D.P. Sanderson, M.B. Tsang, H.M. Xu, S. Pratt, D.E. Fields, K. Kwiatkowski, R. Planeta, V.E. Viola, Jr., and S.J. Yennello, Phys. Rev. Lett. 65, 2114 (1990).

70. Y.D. Kim, R.T. de Souza, D.R. Bowman, N. Carlin, C.K. Gelbke, W.G. Gong, W.G. Lynch, L. Phair, M.B. Tsang, F. Zhu, and S. Pratt, to be published.

71. For our examples, calculations with Eq. 15 ran faster by a factor of about 20 than those with Eq. 1.

Figure Captions

Fig. 1. Comparison of angle-integrated carbon-carbon correlation functions. Calculations with Eq. 1 are shown by points; calculations with the classical approximation, Eqs. 15 and 16, are shown by the curves. The emission times are indicated in the figure.

Fig. 2. Longitudinal and transverse correlation functions for τ=200 fm/c. Longitudinal correlation functions (Ψ=0°-30° or Ψ=150°-180°) are shown by the solid curve and circular points; transverse correlation functions (Ψ=70°-110°) are shown by the dashed curve and square points. Curves show calculations with Eq. 1; points show calculations with Eqs. 5-8, 12-15.

Fig. 3. The points represent correlation functions obtained via trajectory calculations assuming emission from an uncharged source; the curves show the results obtained from Eqs. 15 and 16. The parameters used in these calculations are indicated in the figure.

Fig. 4. Calculations for flat fragment spectra, T=∞, integrated over the indicated momentum intervals. The solid points represent correlation functions obtained via trajectory calculations assuming emission from an uncharged source; the curves show the results obtained from Eqs. 15 and 16; the open points represent three-body Coulomb calculations neglecting recoil effects. The parameters used in these calculations are indicated in the figure.

Fig. 5. Two-fragment correlation functions calculated via three-body trajectory calculations as a function of relative momentum (upper panel) and as a

function of reduced relative velocity, Eq. 18 (bottom panel). Source parameters and atomic numbers of the emitted fragments are indicated in the figure.

Fig. 6. Comparison of two-carbon correlation functions calculated by means of three-body trajectory calculations (points) with correlation functions calculated with Eqs. 15 and 16 (curves). Upper and lower panels show results for total momenta per nucleon of $P/A \leq 110$ MeV/c and $P/A \geq 110$ MeV/c, respectively. The parameters used in these calculations are indicated in the figure.

Fig. 7. Longitudinal and transverse correlation functions between two carbon fragments calculated via trajectory calculations for τ=200 fm/c.

Fig. 8. Two-carbon correlation functions calculated via three-body trajectory calculations for sources of different masses. Solid points: M_S=226 u, open points M_S=10000 u. The upper panel shows calculations for thermal energy spectra and the lower panel shows calculations for flat energy spectra, T=∞, integrated over the indicated energies. The parameters used in these calculations are indicated in the figure.

Fig 1

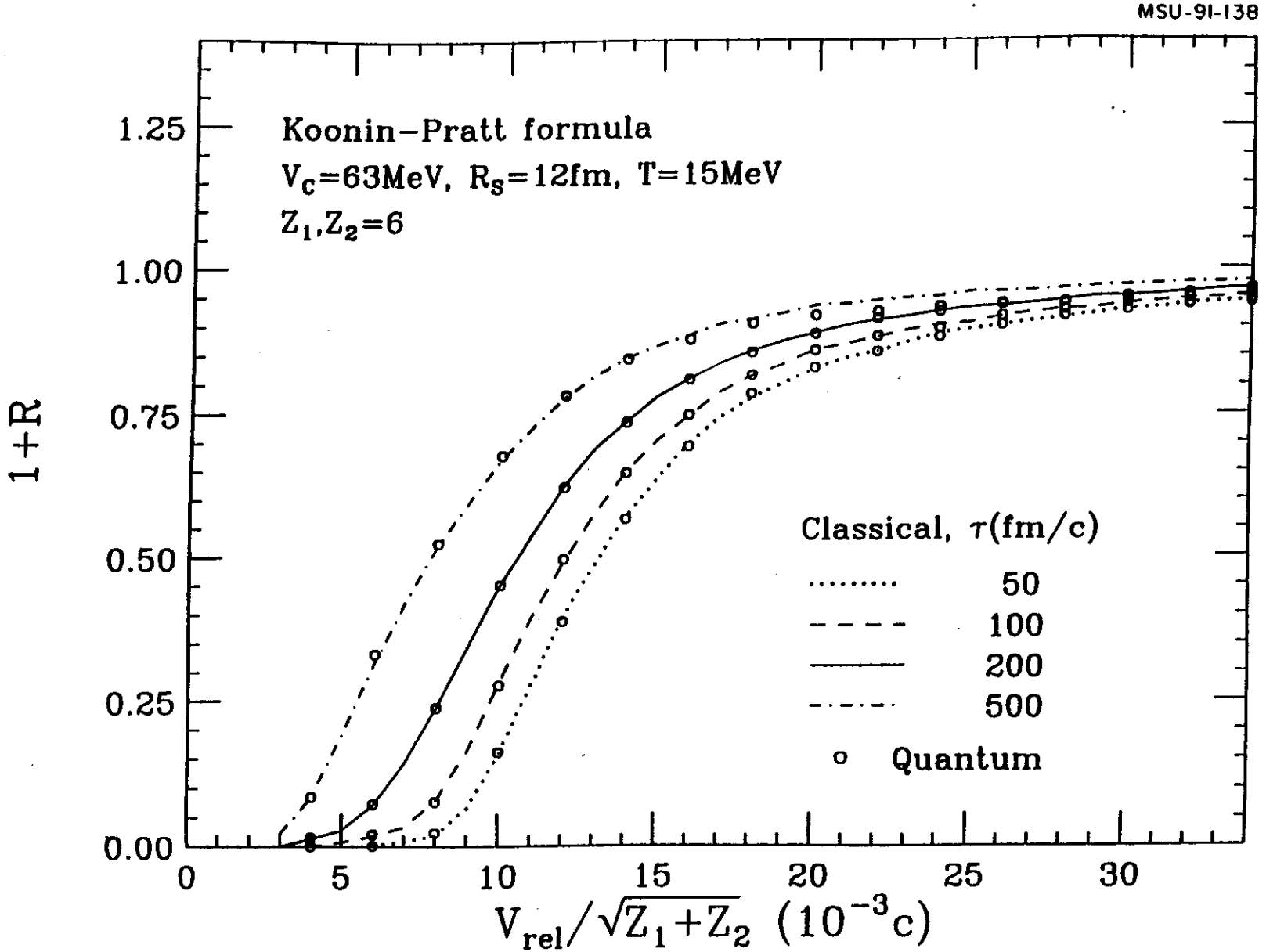
Koonin–Pratt formula
V_c=63MeV, R_s=12fm, T=15MeV
Z_1, Z_2=6
Classical, τ(fm/c)
50
100
200
500
Quantum
1+R
0.00
0.25
0.50
0.75
1.00
1.25
0
5
10
15
20
25
30
$V_{rel}/\sqrt{Z_1+Z_2}$ $(10^{-3}c)$

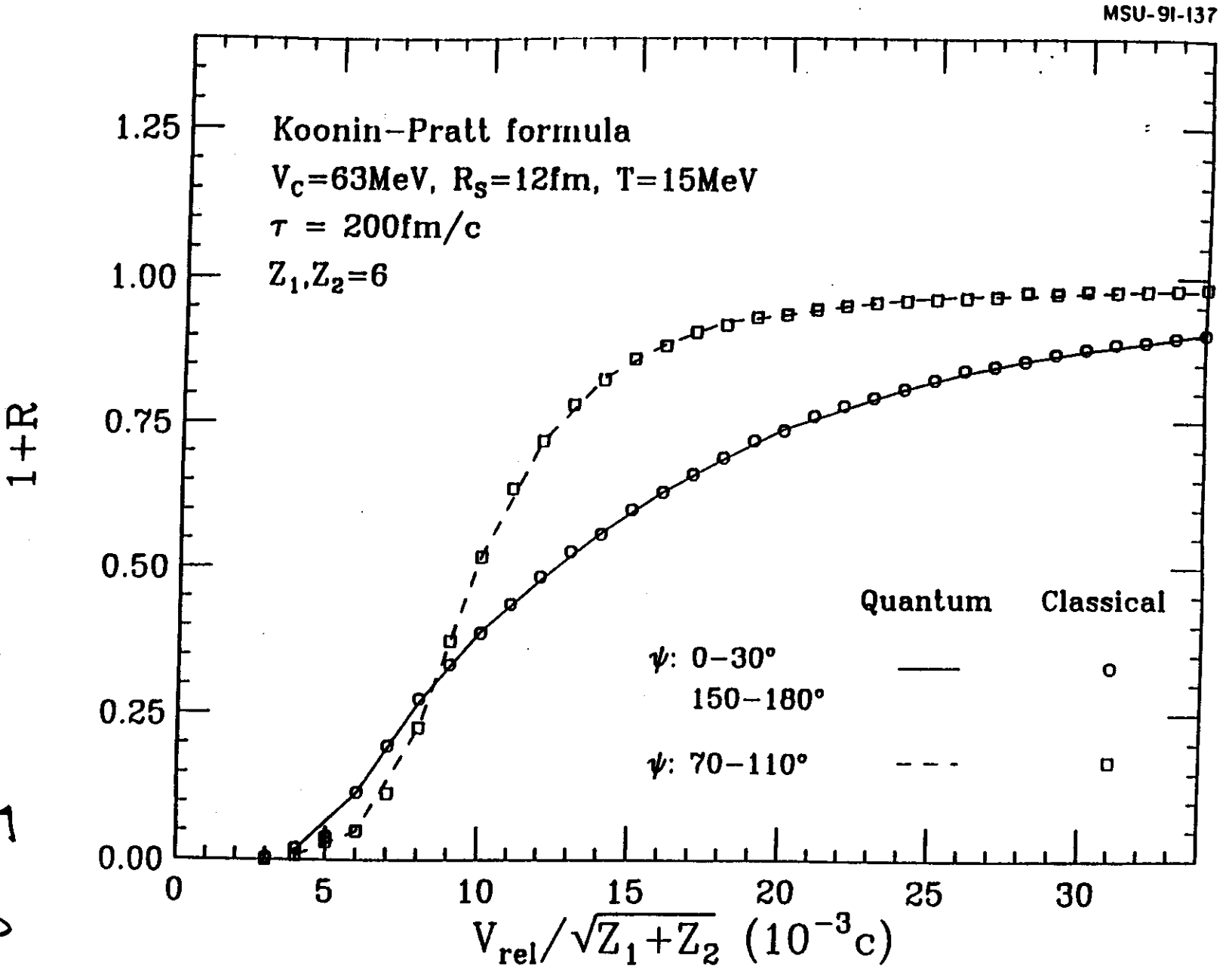
MSU-91-137
Koonin–Pratt formula
V_C=63MeV, R_S=12fm, T=15MeV
τ = 200fm/c
Z_1, Z_2=6
Quantum
Classical
ψ: 0–30°
150–180°
ψ: 70–110°
1+R
$V_{rel}/\sqrt{Z_1+Z_2}$ (10^{-3}c)
0.00
0.25
0.50
0.75
1.00
1.25
0
5
10
15
20
25
30

Fig. 2

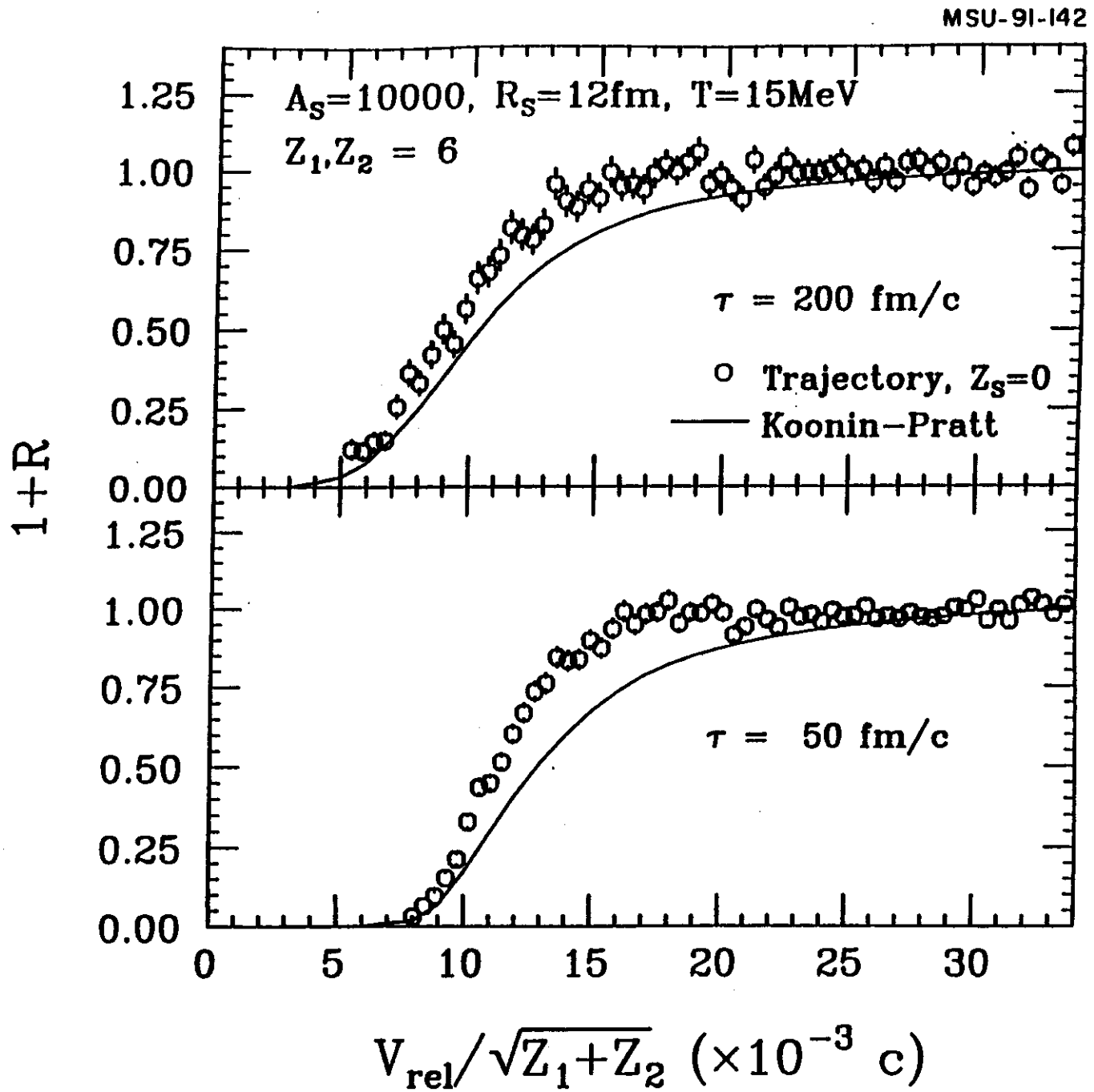
MSU-91-142
A_S=10000, R_S=12fm, T=15MeV
Z_1, Z_2 = 6
τ = 200 fm/c
Trajectory, Z_S=0
Koonin–Pratt
τ = 50 fm/c
1+R
1.25
1.00
0.75
0.50
0.25
0.00
0
5
10
15
20
25
30
$V_{rel}/\sqrt{Z_1+Z_2}$ ($\times 10^{-3}$ c)

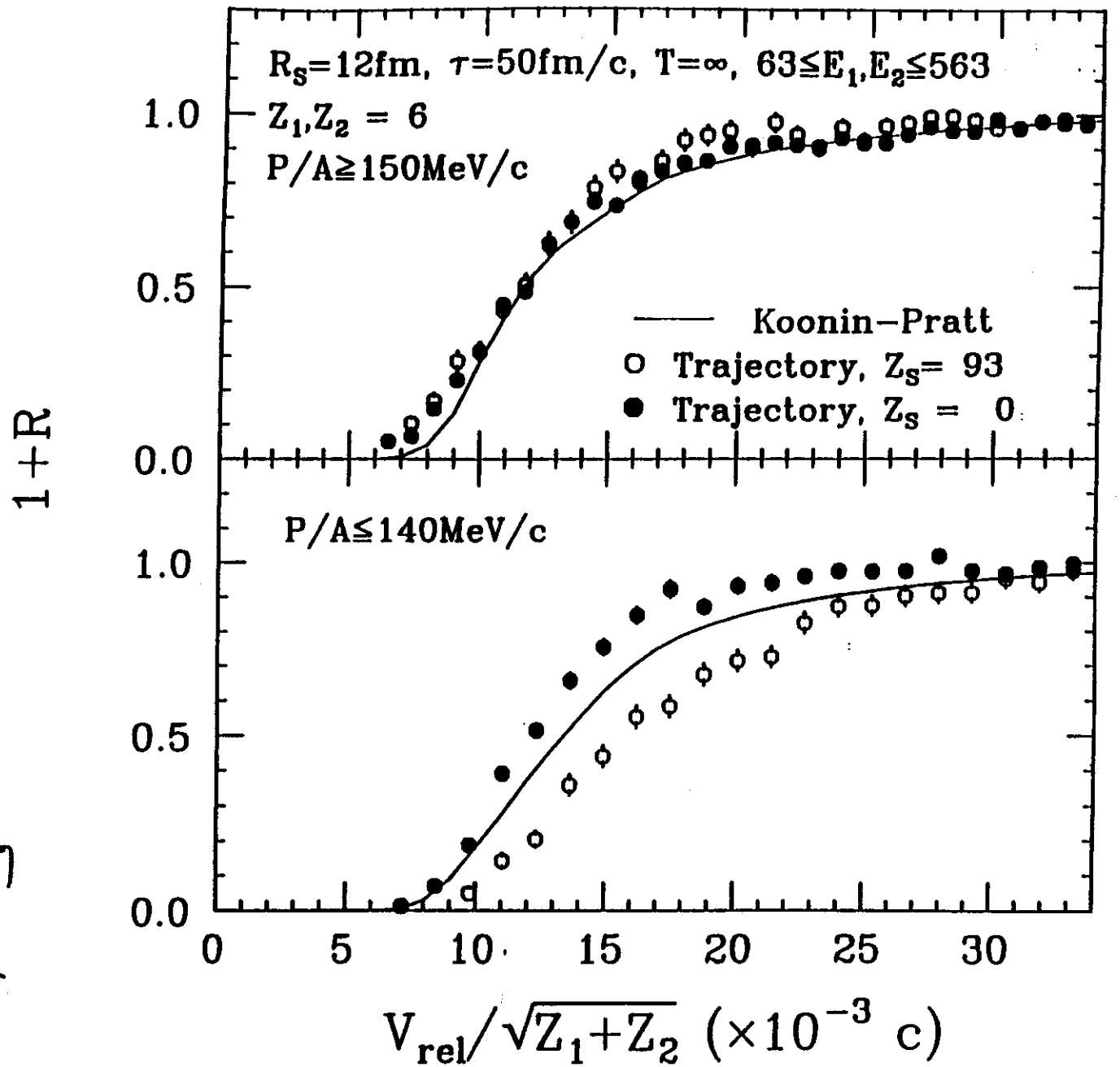
R_S=12fm, τ=50fm/c, T=∞, 63≤E_1,E_2≤563
Z_1,Z_2 = 6
P/A≥150MeV/c
Koonin–Pratt
Trajectory, Z_S= 93
Trajectory, Z_S = 0
P/A≤140MeV/c
1+R
1.0
0.5
0.0
0
5
10
15
20
25
30
$V_{rel}/\sqrt{Z_1+Z_2}$ (×10^{-3} c)

Fig. 4

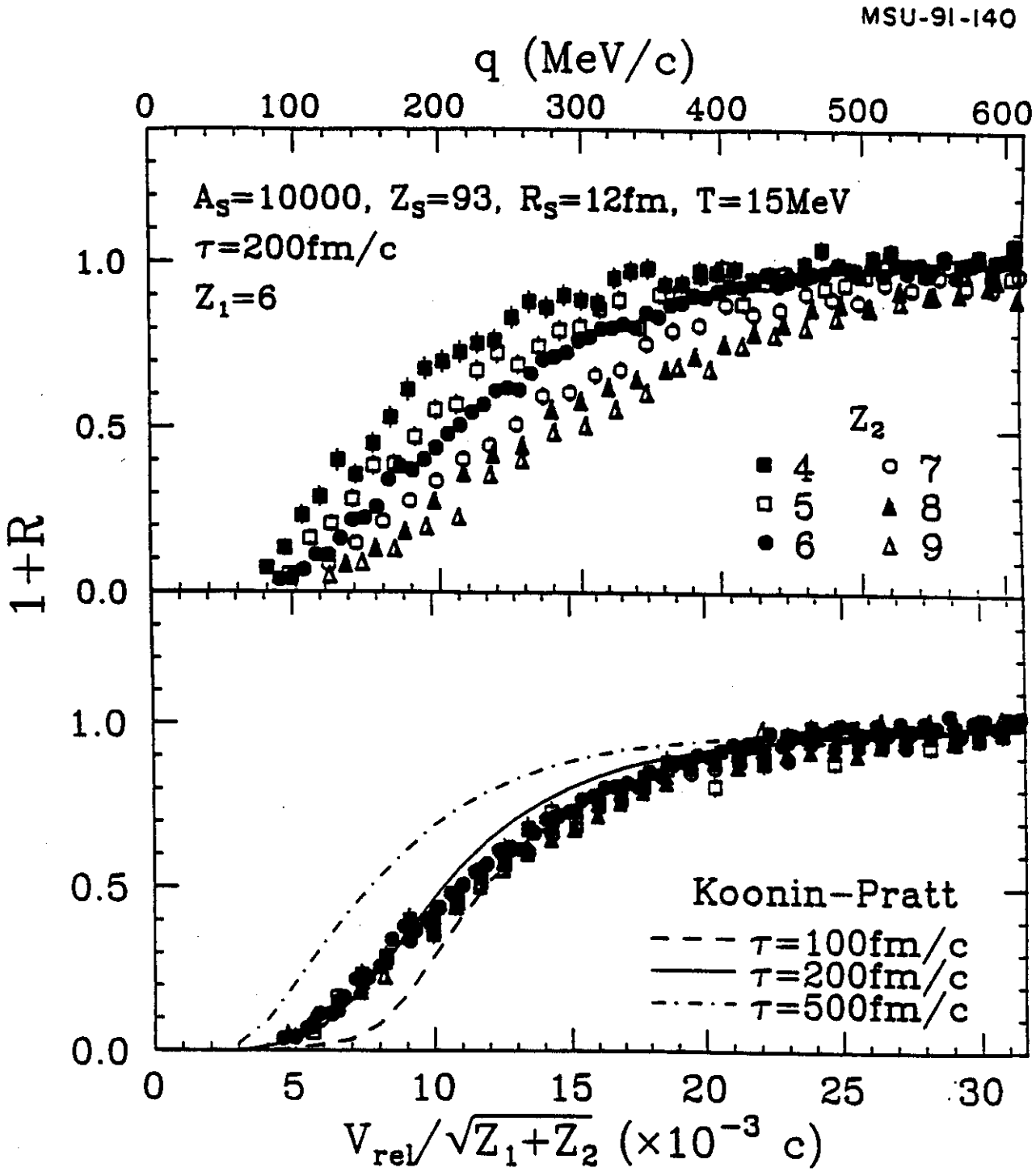
MSU-91-140
q (MeV/c)
0
100
200
300
400
500
600
A_S=10000, Z_S=93, R_S=12fm, T=15MeV
τ=200fm/c
Z_1=6
Z_2
4
5
6
7
8
9
1+R
1.0
0.5
0.0
Koonin-Pratt
τ=100fm/c
τ=200fm/c
τ=500fm/c
0
5
10
15
20
25
30
$V_{rel}/\sqrt{Z_1+Z_2}$ ($\times 10^{-3}$ c)

Fig. 5

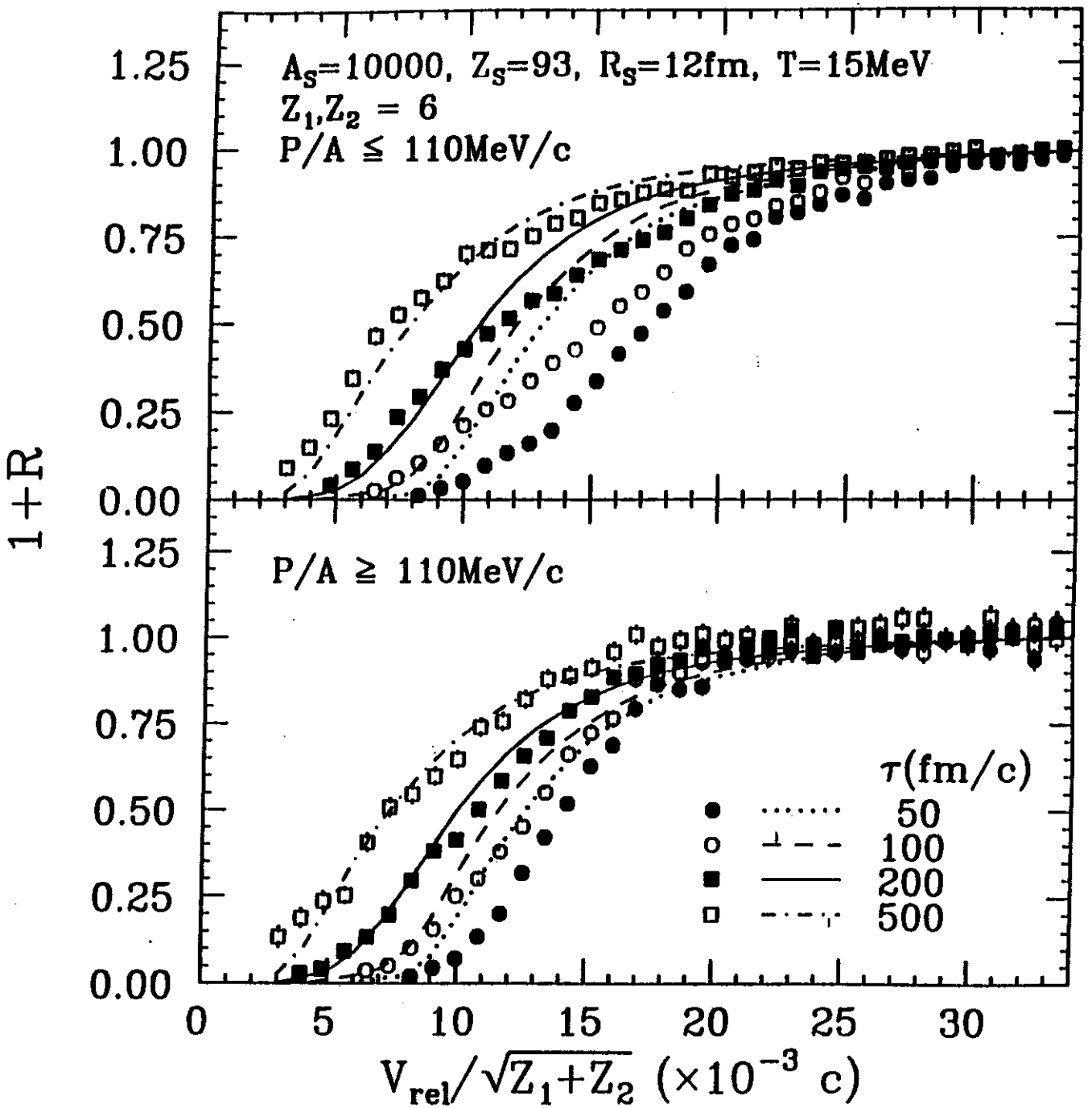
A_S=10000, Z_S=93, R_S=12fm, T=15MeV
Z_1, Z_2 = 6
P/A ≤ 110MeV/c
P/A ≥ 110MeV/c
1+R
$V_{rel}/\sqrt{Z_1+Z_2}$ (×10^{-3} c)
τ(fm/c)
50
100
200
500
0.00
0.25
0.50
0.75
1.00
1.25
0
5
10
15
20
25
30

9.3.1

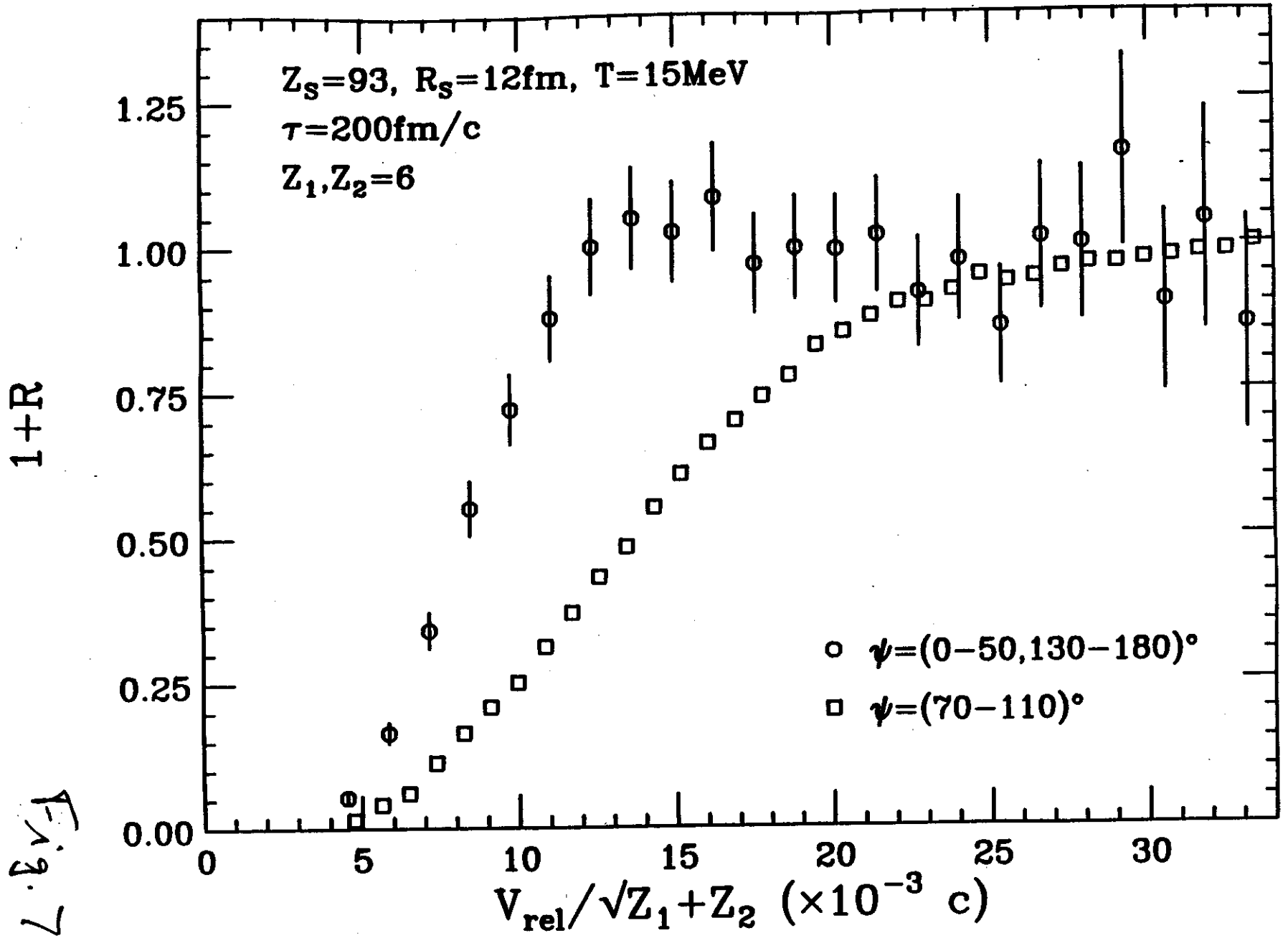
Z_S=93, R_S=12fm, T=15MeV
τ=200fm/c
Z_1,Z_2=6
ψ=(0−50,130−180)°
ψ=(70−110)°
1+R
$V_{rel}/\sqrt{Z_1+Z_2}$ (×10^{-3} c)
0.00
0.25
0.50
0.75
1.00
1.25
0
5
10
15
20
25
30

Fig. 3.7

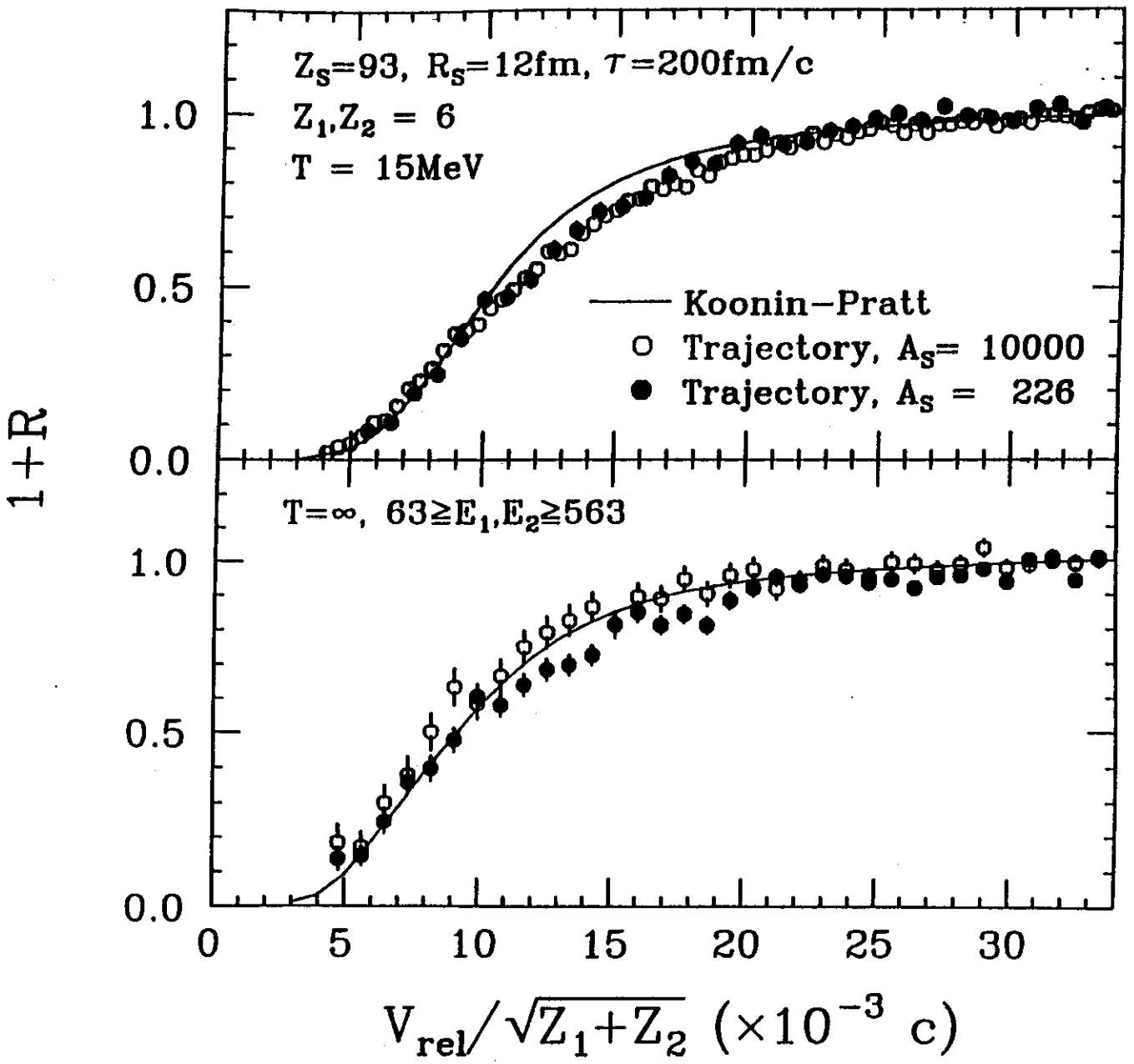
Z_S=93, R_S=12fm, τ=200fm/c
Z_1, Z_2 = 6
T = 15MeV
Koonin–Pratt
Trajectory, A_S= 10000
Trajectory, A_S = 226
T=∞, 63≥E_1, E_2≥563
1+R
1.0
0.5
0.0
0
5
10
15
20
25
30
$V_{rel}/\sqrt{Z_1+Z_2}$ (×10^{-3} c)